Edge impact modeling on stiffened composite structures

Benjamin Ostré, Christophe Bouvet, Clément Minot, Jacky Aboissière

Edge impact modeling on stiffened composite structures

Benjamin Ostré [a], Christophe Bouvet [a,*], Clément Minot [b], Jacky Aboissière [b]

[a] Université de Toulouse; INSA, UPS, Mines Albi, ISAE; ICA (Institut Clément Ader)

ISAE (Institut Supérieur de l'Aéronautique et de l'Espace),
10, avenue Edouard Belin, BP 54032-31055 Toulouse cedex 4, France
[b] SOGETI High Tech, Parc du Millénaire, Bât A1, avenue de l'Escadrille Normandie-Niemen, BP 90076-31703 Blagnac cedex, France

ARTICLE INFO

Keywords:
Carbon fiber
Impact behavior
Finite element modeling
Damage mechanics
Discrete Ply Model

ABSTRACT

Finite Element Analysis of low velocity/low energy edge impact has been carried out on carbon fiber reinforced plastic structure. Edge impact experimental results were then compared to the numerical "Discrete Ply Model" in order to simulate the edge impact damage. This edge impact model is inspired to out-of-plan impact model on a laminate plate with addition of new friction and crushing behaviors. From a qualitative and quantitative point of view, this edge impact model reveals a relatively good experiment/model agreement concerning force–time and force–displacement curves, damage morphology or permanent indentation after impact. In particular the correlation is faithful concerning the results of the parameters retained by industry; the maximum crack length on the edge and the permanent indentation.

Finally, it can be noticed that the model quickly answers in crushing mode and goes in an inadequate way from the dynamic behavior to the quasi-static behavior. In order to correct this problem it seems necessary to implement a strain rate effect in the behavior law on the fiber failure in compression. The next step is to apply this model to the compression after impact.

1. Introduction

Aeronautics integrates many composite structures. Unfortunately, during a manufacturing operation, these structures could be significantly damaged by a foreign object and at the same time the damage occurring might remain undetected by visual inspection [1–4]. Today aeronautical engineering needs to replace metallic materials by composites for weight saving consideration. Metallic materials and their associated plasticity is a well-researched area for many years; however, many such things have to be learnt about composite behavior where the damage prediction remains very challenging [5–8]. A composite center wing box of an airplane is a good example of composite structure with many free edge stringers inside (Fig. 1a). They are extremely loaded and are designed to resist buckling to keep the structure safe, but if a tool drops on the stringer edge during the plane's maintenance, its residual properties can be drastically reduced [4,9,10].

Nowadays, structural stiffeners are mostly used for protection against edge impacts, which needs improvement as additional weight, and is a major concern in aircraft industry. Therefore, it is important to study in detail the edge impact phenomenon and to define the damage scenario, in order to identify the parameters that affect the residual strength after impact. By the way, it will be possible to improve the stringer's impact damage tolerance.

The proof of the impact resistance, depending upon the impact damage detectability, has to be made in order to certify these structures for aeronautical industry, which is the concept of damage tolerance [2,4]. With the help of impact damage tolerance and by defining the damage scenario, it is possible to study and improve the edge impact damage tolerance.

Dent depth and crack length drive the current edge impact detectability threshold criterion for aeronautic fields (Fig. 1b). When the impact indentation is smaller than the barely visible impact damage (BVID) the structure has to support the extreme loads that it is subjected to. However, if the damage is detectable, i.e. when the impact indentation is bigger than the BVID, another criterion must be considered, such as sustain limit loads, repair or change the structure [4].

Composite skin impact issues, and the damage mechanism [1,2,4,11,12] are now fairly well developed. The three types of damages are classically induced on a low-velocity/low-energy impact on a uni-directional (UD) composite laminate: matrix cracking, fiber fracture and delamination [2,10,11]. Matrix cracking conventionally occurs first in the damage scenario. Then, as the

* Corresponding author.
E-mail addresses: christophe.bouvet@isae.fr (C. Bouvet), clement.minot@sogeti.com (C. Minot).

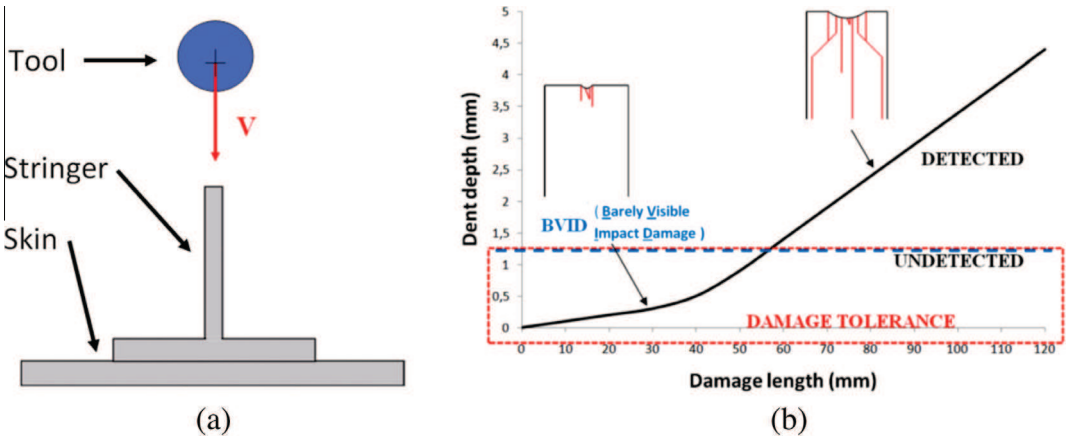

Fig. 1. Edge impact principle (a) and detection policy (b).

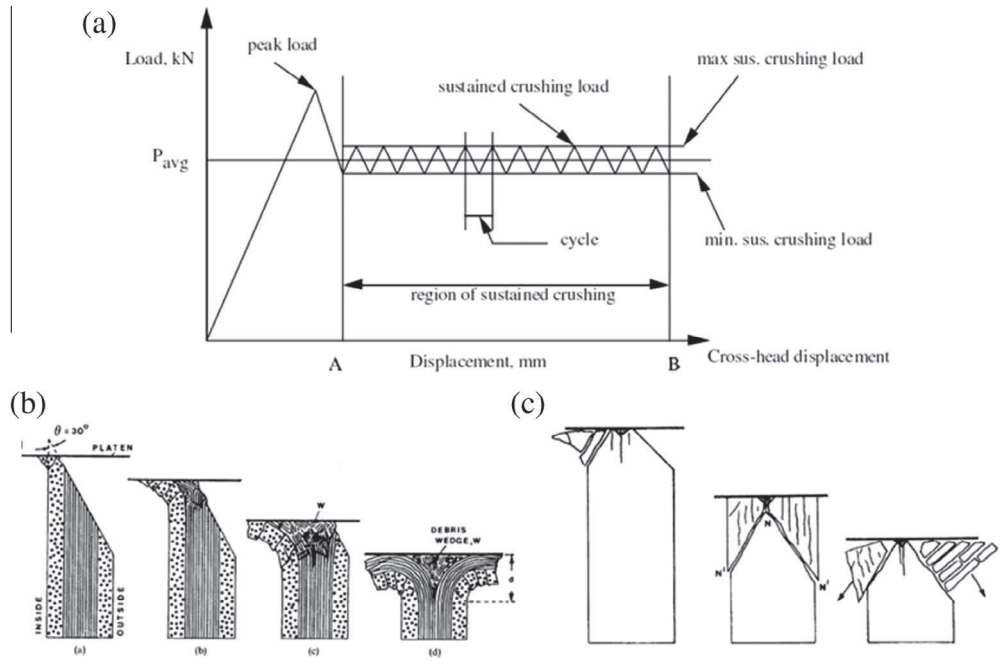

Fig. 2. Crushing test: the typical load–displacement response (a) [13] and the two main degradation modes: splaying (b) and fragmentation (c) [14].

damage grows, delamination quickly occurs. An interaction between these two damage phenomena is also clearly visible during the impact tests [4,10,11].

However, if the focus is shifted from skin to edge, then there seems that the damage tolerance knowledge is missing. As far as the author is concerned, only two researches have been conducted in this regard [9,10], which well elaborate the after impact vulnerability. However, the impact damage scenario is missing to predict an accurate failure by taking into account the physical controlling mechanisms [5]. The understanding and modeling of the edge impact scenario is the key to be able to predict the residual strength, which will be helpful in optimizing composite structures under low-velocity impact. Indeed, some phenomena like compressive fiber failure or wedge effect, which are of minor importance during skin impact, become important in case of edge damage. In addition, the damage scenario of the edge impact test shows similarities with those of the crushing test [13–15], and these studies were the starting point of the edge impact modeling developed in this paper.

The typical load–displacement curve of composite laminate under progressive crushing is shown in Fig. 2a [13,14], where a peak load is generally observed during crushing initiation. After this peak the crushing process turns into progressive crushing that is characterized by a relatively constant force (plateau) with eventual oscillations. This curve is relatively similar to the ones observed during edge impact test [16] (Fig. 20). Hull [14] has classified the crushing process into two main failure modes (Fig. 2b). The first one is known as the splaying mode (Fig. 2a) in which bundles of bending delaminated lamina splay on both sides of a main crack, and the broken fibers and resins trapped at the crushing zone can lead to the formation of debris wedge on the surface of the crushing platen. The second one is called the fragmentation mode (Fig. 2c) in which the plies sustain multiple short length fractures due to pure compression, transverse shearing and sharp

Table 1
T700/M21 mechanical properties.

Carbon/epoxy T700/M21 UD properties		
ep	Ply thickness	0.25 mm
El	Tensile Young's modulus in fiber direction	135 GPa
Ec	Compressive Young's modulus in fiber direction	110 GPa
Et	Transverse Young's modulus	8.5 GPa
Glt	Shear modulus	4.2 GPa
vlt	Poisson's ratio	0.33
Failure		
X_T	Longitudinal tensile strength	2210 MPa
X_c	Longitudinal compressive strength	−1280 MPa
Y_T	Transverse tensile strength	75 MPa
Y_C	Transverse compressive strength	−250 MPa
S	In-plane shear strength	72 MPa

bending, which lead to the formation of small fragments in the crush zone. These two failure modes are also observed during the edge impact test [16].

The aim of this paper is to define an edge impact modeling in order to compare its results with experiments where a vertical drop-weight testing device has been used to perform the edge impacts on different stacking laminates. Precise microscopic examination and X-ray analysis have also been done to closely visualize the damage scenario [16].

2. Experimental study and specimen configuration

First of all, a test specimen has been fabricated to perform preliminary understanding of the phenomenon, which is a representative of the current needs identified above. T700/M21 UD carbon prepreg has been selected, which is a well-known aircraft material [7], and its properties that came from standard tests are listed in Table 1.

The following two different stacking sequences have been studied:

- Stacking A: $[90_2, -45_2, 0_4, 45_2, 0_2]_S$, 6 mm-thick for 24 plies
- Stacking B: $[45_2, 0_2, -45_2, 0_4, 90_2]_S$, 6 mm-thick for 24 plies.

Specimen thicknesses are chosen such as they are consistent with the laboratory test facilities and are also in agreement with the industrial ranges. These stacking sequences are oriented with 50% of 0° plies, which match well with the industrial stacking in such stiffeners. Stacking A is representative of an aeronautical industrial layup (symmetrical, well beaten, no delta at the interface greater than 45°, outside 90° plies to limit 0° plies damage in case of flank impact) and limits the number of interfaces with plies of different orientation, which is important for the modeling phase, and shortens the time required for numerical model calculation. Stacking B follows the same philosophy but has better buckling

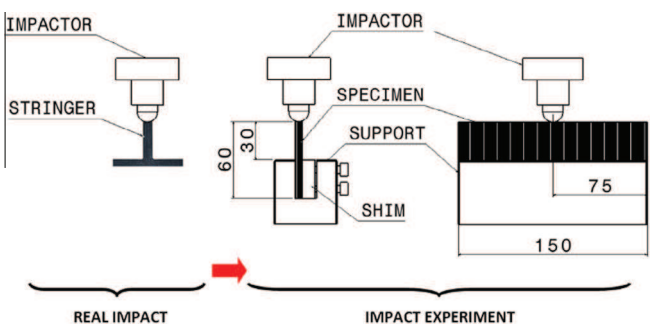

Fig. 3. Edge impact tool principle.

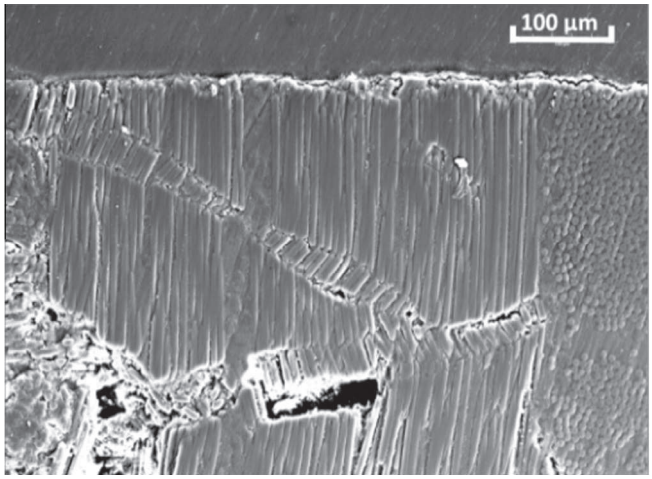

Fig. 4. Kink-bands observed after edge impact (SEM cut section-10 J impact) [16].

resistance due to the outside 45° plies. Finally, the specimen size is representative of a real life stringer structure i.e. 150 mm-long, 60 mm-high with 30 mm-free outside boundary conditions (Fig. 3).

The present work follows a previous experimental study, and in order to help the reader understanding of this paper, the main conclusions of the edge impact experimental study [16] are resumed:

- If fibers are oriented in the impact direction, then kink-bands (Fig. 4) are created (dynamic and static loading).
- In case of the dynamic test, regardless of the energy level (10, 20 or 35 J) and stacking sequence, a specific crushing plateau phenomenon appears. This crushing plateau can be modeled multiplying an average crushing stress of 250 MPa by an average projected area of impact $S_{pi} \approx 25$ mm^2 (Fig. 5). In this case, it can be said that the matrix properties control the crushing plateau.
- Stacking sequence has a relatively small influence on the impact damage, which can be due to the fact that for each stacking presented in this paper [16], proportion of 0° plies is similar.
- For the dynamic impact, irrespective of the energy level and stacking sequence, the force–displacement curves have similar initial stiffness. This initial dynamic force can be evaluated by multiplying the contact surface of each fiber orientation by the fiber compressive failure strength. Therefore, it can be concluded that the fiber properties control the initial impact stiffness (Fig. 5).

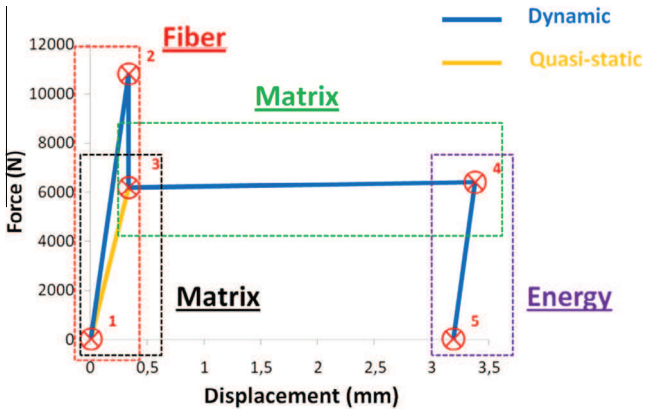

Fig. 5. Analytical approach to understand the impact damage scenario [16].

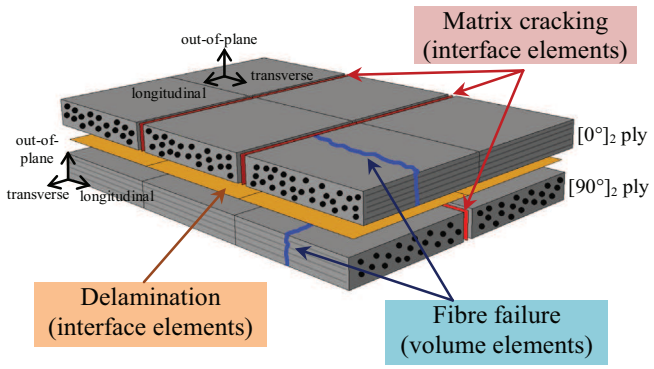

Fig. 6. Modeling of impact damage with the different element types in each oriented ply [17].

- In the quasi-static indentation case, the material is directly crushed. The initial static force can be evaluated by multiplying an average crushing stress of 250 MPa by the projected theoretical surface of the impactor, during the initial phases of the indentation experiment. So, the properties of the matrix control the initial indentation stiffness (Fig. 5).
- There is no equivalence between static/dynamic edge impacts (Fig. 20). During static edge impact, the impactor shape quickly destabilizes the fibers and leads to the development of kink-bands and a crushing phenomenon (Fig. 5).
- The first peak in the indentation force curve is equal to the crushing plateau force value of 6250 N. Furthermore, the behavior after the impactor displacement of 0.5 mm is more difficult to explain. It can be assumed that there is a partial increase of the surface crushing; however, the authors have not verified this hypothesis.

Experimental results presented in [16] will be compared with the results of explicit FE-based simulations in the next paragraph. The FE model consists with interface elements in order to describe the matrix cracks and delamination, and volume elements in order to predict the fiber failure. Correct FE models will be good substitute for expensive experiments and thus shortening the development time of improved composite structures.

3. Numerical modeling

Hongkarnjanakul et al. [17,18] presented a discrete 3D impact model using Abaqus explicit solver and a user-defined Vumat subroutine. In the model, the three major failure modes observed in composite impact tests were considered: the intra-ply matrix cracking, the inter-ply delamination and the intra-ply fiber failure (Fig. 6). Nevertheless in order to simulate loadings such as edge impact or crushing, the crushing process should be taken into account. Indeed such tests induce high compressive loading leading to crushing process and to high compressive strains in the transverse and longitudinal directions. In the next paragraph, the "Discrete Ply Model" (DPM) will be presented and the crushing modeling will be particularly focused. Firstly the behavior in the transverse direction, i.e. the matrix cracking and the transverse crushing, will be presented. Afterwards the delamination modeling will be briefly reminded; interface elements with cohesive zone [19] are classically used. Lastly the behavior in the longitudinal direction, i.e. the fiber failure and the longitudinal crushing, will be presented.

3.1. Modeling in the transverse direction

Matrix cracking is taken into account in the DPM using interface element normal to the transverse direction (Fig. 6). The onset of damage of these interface elements is based on Hashin's theory [20]. The Hashin's criteria is calculated in the neighboring volume elements (for more details, see [17]) to avoid stress singularities at the matrix cracking crack tip:

$$\left(\frac{\langle \sigma_t \rangle^+}{\sigma_t^{f,t}}\right)^2 + \frac{\tau_{lt}{}^2 + \tau_{tz}^2}{\tau_{lt}^{f^2}} = 1 \tag{1}$$

where σ_t, τ_{lt} and τ_{tz} are respectively the transverse stress, the shear stress in the (l, t) plane and the shear stress in the (t, z) plane, evaluated in the neighboring volume elements, $\sigma_t^{f,t}$ the transverse failure stress in tension and τ_{lt}^f the failure shear stress [18].

This criterion is assessed at each time increment and the interface stiffness becomes zero if the criterion is reached, i.e. the matrix develops cracks, and remains intact in otherwise. The initial stiffness of the interface element is chosen very high, typically 10^6 MPa/mm.

As previously mentioned, the transverse crushing must be taken into account. Israr et al. [15] showed that during crushing process, the crushing stress is about constant (Fig. 20) and its value is similar to the compressive matrix failure stress. Then a crushing plateau is applied in transverse direction (Fig. 7) in order to represent, at the same time, the compressive matrix failure and the crushing in this direction.

Moreover, to simulate the plastic deformation ε_t^{pl} due to transverse crushing, a plastic behavior is imposed using a yield function f_t:

$$\varepsilon_t^{pl} \text{ such as } f_t = |\sigma_t - \sigma_t^{crush}| \leqslant 0 \tag{2}$$

where σ_t^{crush} is the crushing stress and the transverse stress σ_t is evaluated using:

$$\begin{aligned}\sigma_t = {} & H_{lt} \cdot (1 - d_f) \cdot (\varepsilon_l - \varepsilon_l^{pl}) + H_{tt} \cdot (1 - d_f) \cdot (\varepsilon_t - \varepsilon_t^{pl}) \\ & + H_{tz} \cdot (1 - d_f) \cdot (\varepsilon_z - \varepsilon_z^{pl})\end{aligned} \tag{3}$$

where H_{lt}, H_{tt} and H_{tz} are the elasticity stiffness, ε_l (ε_z) the longitudinal (out-of-plane) strain, d_f the damage in the fiber direction and ε_l^{pl}, ε_t^{pl}, ε_z^{pl}, the plastic strain respectively in the l, t and z-directions. The fiber damage d_f and the plastic longitudinal strain ε_l^{pl} will be explain in the next paragraph, and the plastic out-of-plane strain ε_z^{pl} is due to the expansion in the z-direction due to crushing in the transverse direction considering a constant volume:

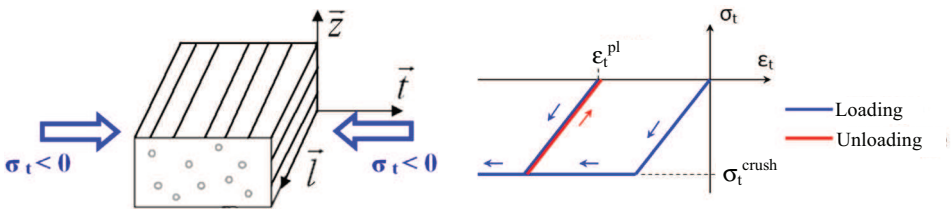

Fig. 7. Crushing principle in the t direction.

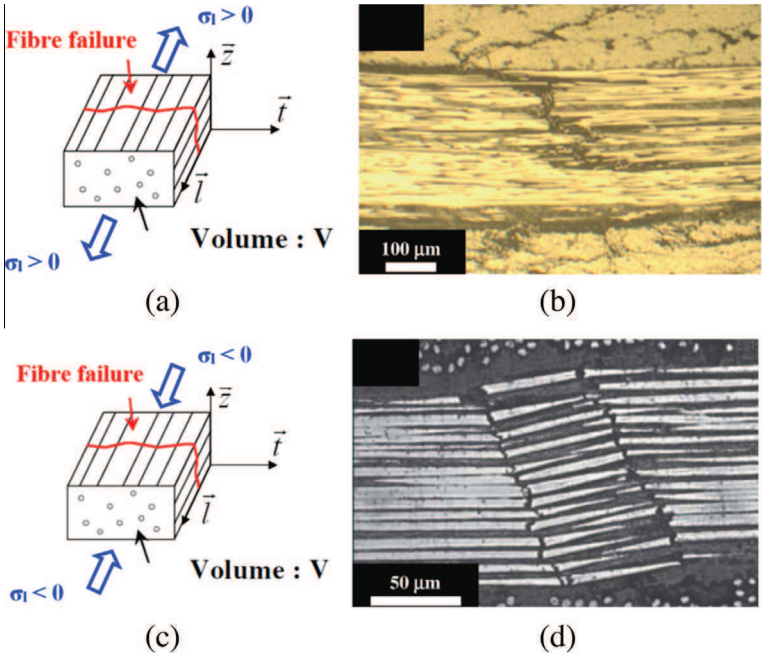

Fig. 8. Fiber failure in tension (a) and corresponding cut section after impact in carbon–epoxy laminate (b) [23]; and fiber failure in compression (c) and corresponding cut section after impact in a carbon–epoxy laminate (d) [23].

$$\dot{\varepsilon}_z^{pl} = -\dot{\varepsilon}_t^{pl} \tag{4}$$

This relation makes possible the coupling between the transverse and out-of-plane directions during a *t*-crushing. In parallel, it would be necessary to consider a crushing in the *z*-direction and to take into account the coupling between these 2 crushings. This work has not been done so far because the *z*-crushing is not present in the edge impact. Moreover the coupling between the transverse crushing and the fiber crushing is not considered due to the lack of data and because it is not considered of first importance. The fiber crushing will be explained in the next paragraph and will allow determining of ε_l^{pl}.

In fact the coupling between plastic strains in *t* and *z*-directions (Eq. (4)) could lead to high positive strain in the out-of-plane direction and to increasing of the crushing stress σ_t^{crush}. But the results of Israr et al. [15] showed that during crushing process, the crushing stress is about constant, then it is necessary to take into account this expansion to define the *t*-crushing stress:

$$\sigma_t^{crush} = \frac{\sigma_t^{f,c}}{\lambda_z^{pl}} \tag{5}$$

where $\sigma_t^{f,c}$ is the transverse failure stress in compression and λ_z^{pl} the plastic elongation in the *z*-direction. This elongation λ_z^{pl} makes it possible to take into account the variation of the element size according to *z* and represents the increase (if it is higher than 1) of plastic size, that is to say the *z*-size increase corresponding to the *t*-crushing. This increase is due to remaining debris; therefore it cannot physically increase the crushing force. This expansion is obtained by integrating the plastic deformation according to *z*:

$$\dot{\lambda}_z^{pl} = \lambda_z^{pl} \cdot \dot{\varepsilon}_z^{pl} \tag{6}$$

In the initial position, λ_z^{pl} is obviously equal to 1 and can only increase because ε_t^{pl} is negative due to crushing and then ε_z^{pl} is positive due to the coupling (Eq. (4)).Moreover in order to limit the excessive expansion due to crushing process, λ_z^{pl} is averaged on each volume element and is limited at a maximum value:

$$\begin{cases} \lambda_z^{pl} = \underset{i=1,8}{\text{average}}\ \lambda_z^{pl}(i) \\ \lambda_z^{pl} = \min\left(\lambda_z^{pl}, \lambda^{\max}\right) \end{cases} \tag{7}$$

where $\lambda_z^{pl}(i)$ is the plastic out-of-plane elongation of the *i*th integration point, considering the volume elements are C3D8 with 8 integration points, and $\lambda^{\max}$ is the maximum plastic out-of-plane elongation taken equal to 2 in this study. In the same way, in order to avoid excessive distortion of volume elements the plastic strains are limited to a minimum value $\varepsilon^{\min}$. To do that, the crushing stress σ_t^{crush} is increased with exponential function versus plastic strain:

$$\text{If } \varepsilon_t^{pl} < \varepsilon^{\min} \text{ then } \sigma_t^{crush} = \frac{\sigma_t^{f,c}}{\lambda_z^{pl}} \cdot \exp\left(-k \cdot \left(\varepsilon_t^{pl} - \varepsilon^{\min}\right)\right) \tag{8}$$

where *k* is taken high enough, usually equal to 2, and $\varepsilon^{\min}$ is usually taken equal to −1.6, that is to say to approximately 80% of the initial height. Of course, in order to simulate higher crushing process, it should be necessary to remove volume element. But in the present

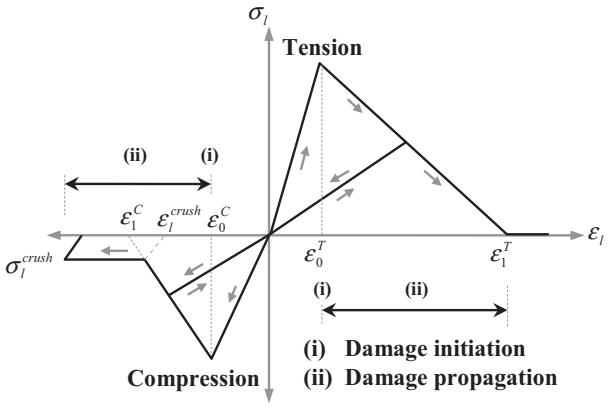

Fig. 9. Behavior law of the fiber in the longitudinal direction in tension and compression with damage initiation and propagation [17].

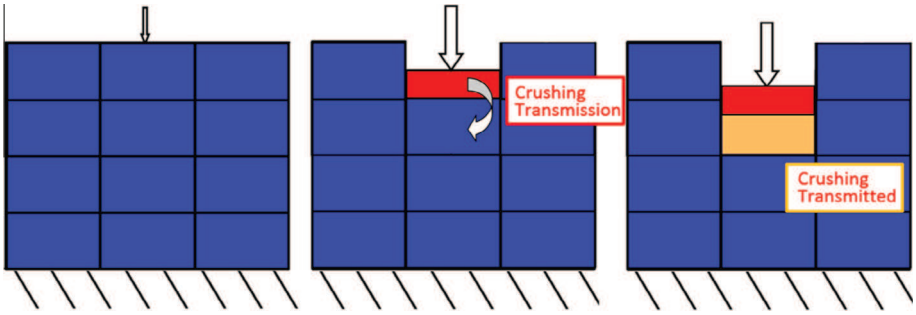

Fig. 10. Crushing transmission principle.

case, this phenomenon is not considered of first importance and is not taken into account.

Then permanent indentation is managed in the matrix cracking elements. Indeed, a large part of the permanent indentation seems to come from remaining debris in cracks oriented at 45° in the ply thickness [7]. This phenomenon is taken into account in the matrix cracking elements applying a «pseudo-plastic» behavior with σ_t in tension and in shear with τ_{tz} in order to limit the no-closure of a crack at 45° in the (t, z) plan after failure. This part of the modeling is not developed in this article but the interested reader can obtain details in [15].

Permanent indentation plays a crucial role in the detection of the damage and aeronautical certification damage tolerance policy [1,4,8,9,11,21]. Permanent indentation is thus very important in FE analysis. Furthermore, a large part of this indentation is due to crushing in l and t-directions.

3.2. Modeling of delamination

Delamination damage consists with important cracks between plies. It is typically modeled with cohesive interface elements based on fracture mechanics [19,22]. This modeling choice makes it possible to correctly take experimental observations into account and has been adopted in this study. Then after the different plies are meshed with volume elements and matrix crack interface elements, two consecutive plies are joined using zero-thickness interface elements (Fig. 6). These delamination interface elements are written in mixed fracture mode (mode I, II, III) to simulate the energy dissipated by delamination. Moreover the shearing (II) and tearing (III) fracture modes are combined and mode II is supposed equal to mode III. And in order to represent the overlap of 2 consecutive plies, the 0° and 90° plies are meshed with square elements and the 45° and −45° plies are meshed with diamond-shaped elements [17]. Moreover, a linear criterion is used:

$$\frac{G_I}{G_I^c} + \frac{G_{II}}{G_{II}^c} + \frac{G_{III}}{G_{III}^c} = 1 \tag{9}$$

where G_I^c, G_{II}^c and G_{III}^c represent the critical energy release rate (ERR) of delamination in mode I, II and III, respectively. Then, thanks to energy dissipation of fracture mechanics, the delamination criteria presents a classical behavior of the cohesive zones with a linear propagation of the stress function of the displacement [19,22].

3.3. Modeling in the longitudinal direction

The fiber failure plays a great role on the impact damages and on the crushing (Fig. 8) [5,13–15] and should be taken into account. Due to the high critical ERR of fiber failure [23], it is necessary to dissipate this energy in the model. Additional interface elements could be used but would result in very complex meshing. Therefore, to avoid the use of such interfaces, fiber failure is taken into account using conventional continuum damage mechanics but with original formulation between the integration points of the element to produce a constant ERR per unit area. This approach can be compared to methods based on characteristic element length which makes possible mesh-size independent modeling [23–25].

Therefore, to be able to produce the critical ERR due to fiber fracture per unit area of crack [5,7,23–25], the behavior laws of the 8 integration points of a volume element are managed together. In this case, the law is written only in opening mode I, but could be generalized with other fracture modes:

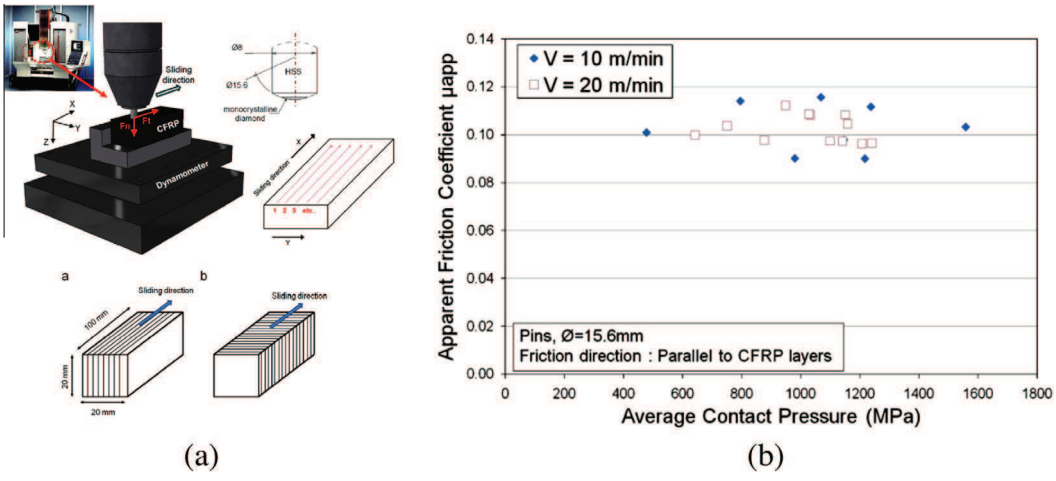

Fig. 11. Machining friction (a) and friction coefficient observed during tests (b) [26].

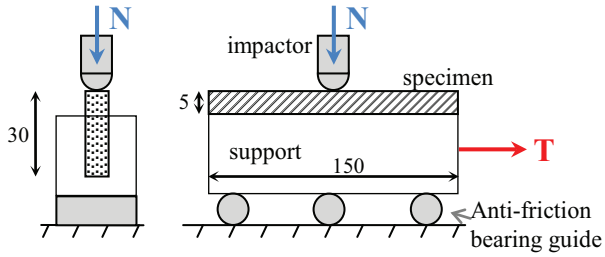

Fig. 12. Friction experiment principle.

$$\int_V \int_0^{\varepsilon_1} \sigma_l \cdot d\varepsilon_l \cdot dV = S \cdot G_l^f \tag{10}$$

where σ_l is the longitudinal stress, V the volume of the element, S the section normal to the fiber direction l, ε_l the total strain degradation of the fiber stiffness and G_l^f the critical ERR in opening mode in the fiber direction (Fig. 9). Then the fiber stiffness is classically degraded by using a damage variable d_f. This damage variable is conventionally calculated compared to the longitudinal strain with the aim to obtain a linear decrease of the longitudinal stress:

$$d_f = \frac{\varepsilon_1^{T \text{ or } C} \cdot (\varepsilon_l - \varepsilon_0^{T \text{ or } C})}{\varepsilon_l \cdot (\varepsilon_1^{T \text{ or } C} - \varepsilon_0^{T \text{ or } C})} \tag{11}$$

where ε_0^T (ε_0^C) is the starting strain degradation of the fiber stiffness in tension (compression) and ε_1^T (ε_1^C) the total strain degradation of the fiber stiffness in tension (compression).

Obviously the critical ERR is different under tension or compression loading [15,23,24] because the failure phenomena are different: a classic fiber failure is observed under tension loading (Fig. 8b) and kink-bands are observed under compression loading (Fig. 8d) [23]. Then it is necessary to take into account these 2 phenomena and to apply a coupling because it is possible to observe fiber failure in compression and in tension at the same time in the 8 integration points of the same volume element. It is for example the case if the volume element is submitted to bending loading. Moreover due to the lack of data on this coupling, a tension/compression linear coupling is applied:

$$\frac{G_l^t}{G_l^{f,t}} + \frac{G_l^c}{G_l^{f,c}} = 1 \tag{12}$$

With:

$$\text{If } \varepsilon_l > 0 \text{ then } \begin{cases} G_l^t = \frac{1}{S} \cdot \int_V \int_0^{\varepsilon_1^T} \sigma_l \cdot d\varepsilon_l \cdot dV \\ G_l^c = 0 \end{cases} \tag{13}$$

$$\text{If } \varepsilon_l < 0 \text{ then } \begin{cases} G_l^t = 0 \\ G_l^c = \frac{1}{S} \cdot \int_V \int_0^{\varepsilon_1^C} \sigma_l \cdot d\varepsilon_l \cdot dV \end{cases} \tag{14}$$

where $G_l^{f,t}$ ($G_l^{f,c}$) is the critical ERR in tension (compression). These equations (Eqs. (12)–(14)) makes it possible to determine ε_l^T and ε_l^C and the Eq. (11) makes it possible to evaluate the fiber damage d_f. Then the longitudinal stress in tension is calculated as:

If $\varepsilon_l > 0$ then

$$\begin{aligned} \sigma_l = {} & H_{ll}^t \cdot (1 - d_f) \cdot \varepsilon_l + H_{lt} \cdot (1 - d_f) \cdot (\varepsilon_t - \varepsilon_t^{pl}) \\ & + H_{lz} \cdot (1 - d_f) \cdot (\varepsilon_z - \varepsilon_z^{pl}) \end{aligned} \tag{15}$$

where H_{ll}^t is the elasticity stiffness in the longitudinal direction in tension which is different of this one in compression H_{ll}^c. If the longitudinal strain is negative, the problem is more complex because it is necessary to distinguish the fiber behavior before and after crushing. Before the crushing the stress is evaluated similarly to the tension case:

If $\varepsilon_l < 0$ and before crushing then:

$$\begin{aligned} \sigma_l = {} & H_{ll}^c \cdot (1 - d_f) \cdot \varepsilon_l + H_{lt} \cdot (1 - d_f) \cdot (\varepsilon_t - \varepsilon_t^{pl}) \\ & + H_{lz} \cdot (1 - d_f) \cdot (\varepsilon_z - \varepsilon_z^{pl}) \end{aligned} \tag{16}$$

But when the crushing starts, i.e. when the strain ε_l reaches the crushing strain ε_l^{crush} for the first time, a plastic longitudinal strain ε_l^{pl} is added and the stress is evaluated as:

If $\varepsilon_l < 0$ and after crushing then:

$$\begin{aligned} \sigma_l = {} & H_{ll}^c \cdot \left(\varepsilon_l - \varepsilon_l^{pl}\right) + H_{lt} \cdot (1 - d_f) \cdot \left(\varepsilon_t - \varepsilon_t^{pl}\right) \\ & + H_{lz} \cdot (1 - d_f) \cdot \left(\varepsilon_z - \varepsilon_z^{pl}\right) \end{aligned} \tag{17}$$

The problem of this formulation is to induce a discontinuity of the plastic strain ε_l^{pl} at the moment of the crushing starting: the plastic strain is null before crushing and reaches the crushing strain ε_l^{crush} when the crushing starts. This point will have to be focused and a solution could be to manage the fiber damage in compression using a plastic strain ε_l^{pl} in spite of the damage parameter d_f. This work is in progress.

Moreover as the crushing process in longitudinal direction is supposed independent of the matrix crushing process (in t and

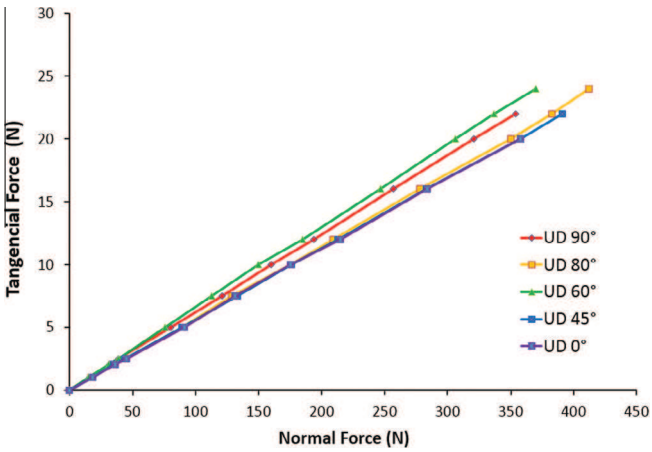

Fig. 13. Friction experiment: normal force versus tangential force.

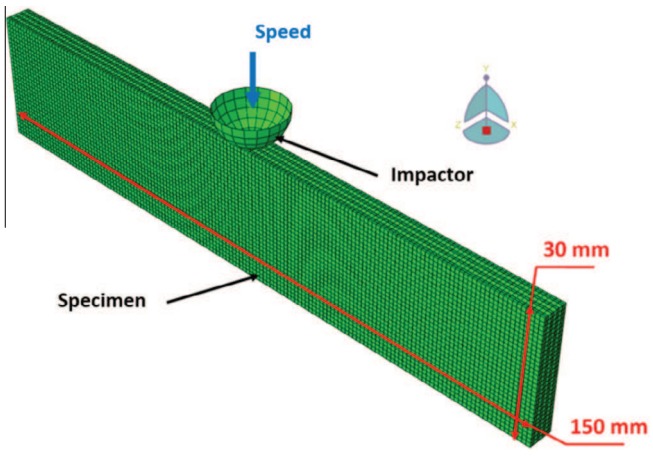

Fig. 14. Edge impact model principle.

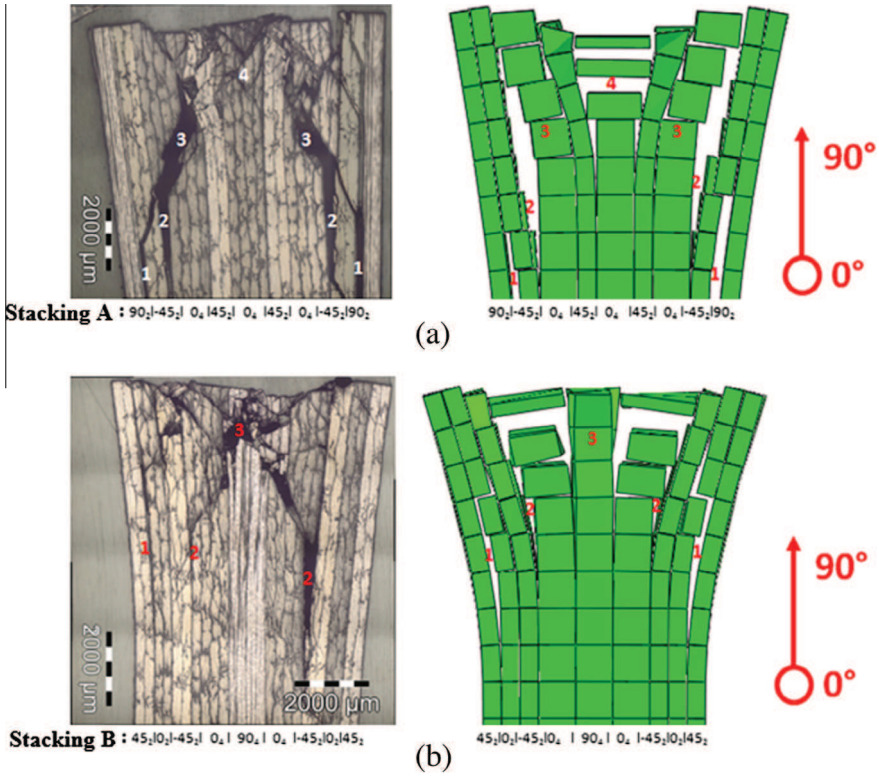

Fig. 15. Experiment/model comparison of cut sections of stacking A (a), and B (b) impacted at 10 J just under the impactor.

z-directions), the crushing stress σ_l^{crush} is supposed constant and equal to the matrix failure stress:

$$\sigma_l^{crush} = \sigma_t^{f,c} \tag{18}$$

It means in particular that the mean crushing stress is supposed the same in longitudinal and in transverse direction, as shown by Israr et al. [15]. This result is very surprising and is difficult to explain, and until now is only the result of experimental tests [15]. In the future it will be necessary to focused on this problem, and perhaps if it is necessary, to use different values of crushing stress in the longitudinal and in the transverse direction.

Finally the plastic strain ε_l^{pl} can be determined using a yield function f_l and the corresponding crushing stress:

$$\varepsilon_l^{pl} \text{ such as } f_l = |\sigma_l - \sigma_l^{crush}| \leqslant 0 \tag{19}$$

And contrary to the transverse direction, no coupling is considered between the longitudinal plastic strain and the transverse and out-of-plane plastic strains. This means the different crushing processes in the fiber direction and in the (t, z) plane are supposed totally independent. Of course this hypothesis should be confirmed by specific experimental tests and this assumption must be questioned if necessary.

It could be also noticed that with this approach the other fiber failure modes (II and III) are not taken into account because data are missing and they are judged of secondary importance [18]. Moreover if a laminate is subjected to shear loading, in some cases, the matrix is quickly damaged and once the fibers are degraded they are "dry" and are thus mainly subjected to tension loading.

The last step to achieve to correctly simulate the crushing is to transmit the crushing information between consecutive elements in the longitudinal direction. In the same way than Israr et al. [15], when the crushing is reached, the crushing is transmitted (Fig. 10) to the two neighboring elements (or with the neighbor element if it is an edge element). Indeed once the crushing process is initiated, the neighboring elements cannot reach any more the failure compression stress according to longitudinal direction, nor to dissipate $G_l^{f,c}$.

In the same way than the transverse crushing, in order to avoid excessive distortion of volume elements, the longitudinal plastic strain is limited to a minimum value $\varepsilon^{\min}$. To do that, the crushing stress σ_l^{crush} is increased with exponential function versus plastic strain:

$$\text{If } \varepsilon_l^{pl} < \varepsilon^{\min} \text{ then } \sigma_t^{crush} = \sigma_t^{f,c} \cdot \exp\left(-k \cdot \left(\varepsilon_l^{pl} - \varepsilon^{\min}\right)\right) \tag{20}$$

where k is taken high enough, usually equal to 2, and $\varepsilon^{\min}$ is usually taken equal to -1.6, that is to say to approximately 80% of the initial height.

3.4. Conclusion on the modeling

This model based on DPM makes it possible to take into account the loss of stiffness of the specimen due to the impact damage and the delaminated surfaces shape [17,18]. In particular, the good correlation between the delaminated surfaces shape obtained in experiments, which is however very complex and characteristic of the impact damage, allows to show that the model of interaction between matrix cracking and delamination seems correct. Nevertheless this model must be still tested on other impact configurations, such as other stacking or boundary conditions.

In particular the integration of the crushing, which is done in this paper, is the first step to generalize the DPM to severe solicitations. Of course this work is only a preliminary job and some hypotheses should be detailed and confirmed, or abandoned if it proves to be wrong. In particular these points should be focused and discussed:

- The out-of-plane crushing is not simulated because it is considered of second importance for the edge impact.
- The transverse crushing is supposed to create expansion only in the out-of-plane direction.
- Only the first mode of fiber failure is taken into account.
- The coupling between crushing in fiber direction and crushing in the plane normal to the longitudinal direction is neglected. In particular the expansion in the transverse and out-of-plane directions due to longitudinal crushing is not taken into account and vice versa.
- The compressive fiber failure is simulated using a damage parameter and the corresponding crushing by a plastic model; these two approaches could be mixed.

4. Edge impact model results

An important point of the edge impact is the friction between the impactor and the specimen. Indeed the friction influences the opening of the composite plate during the edge impact and then should be studied. An experimental test has been carried out in order to measure the friction coefficient under conditions representative of the edge impact test [16].

4.1. Friction test

Some studies on the friction between steel and composite were already carried out in the literature [26,27]. A particularly interesting study (Fig. 11) was carried out on friction between a machining tool and a laminate carbon [26].

The major result of this study lies in the relatively low friction coefficient observed during the experiment (Fig. 15b) from approximately 0.1. In order to benchmark this value, a friction test was carried out on a 100 kN electro-mechanics Instron machine (Fig. 12).

The experimental set-up consists with a composite specimen glued on a support translational with the frame. A normal force is imposed using a 16 mm-diameter spherical impactor on the composite specimen and the force necessary to move the support is measured (Fig. 12).

A UD plate was manufactured with all the plies directed in the same direction: $[0_{30}]$, that is to say a 7.5 mm-thickness for 30 plies of T700/M21 carbon UD prepreg. Five specimens are then cut out with five fiber orientations: $[0_{30}]$, $[45_{30}]$, $[60_{30}]$, $[80_{30}]$ and $[90_{30}]$. This study makes it possible to study the impactor/specimen friction according to the fiber orientation. Finally specimen dimensions are 150 mm-length, 30 mm-height including 5 mm out of the boundary conditions. The tests are carried out dry, i.e. without oil or grease.

A normal effort N is applied to the specimen using the 16 mm-diameter spherical impactor of the edge impact test. A guide with bearing is positioned between the specimen and the frame to leave free the specimen translation. Then the tangential force T is increased until reaching the slip which makes possible to obtain the friction coefficient f:

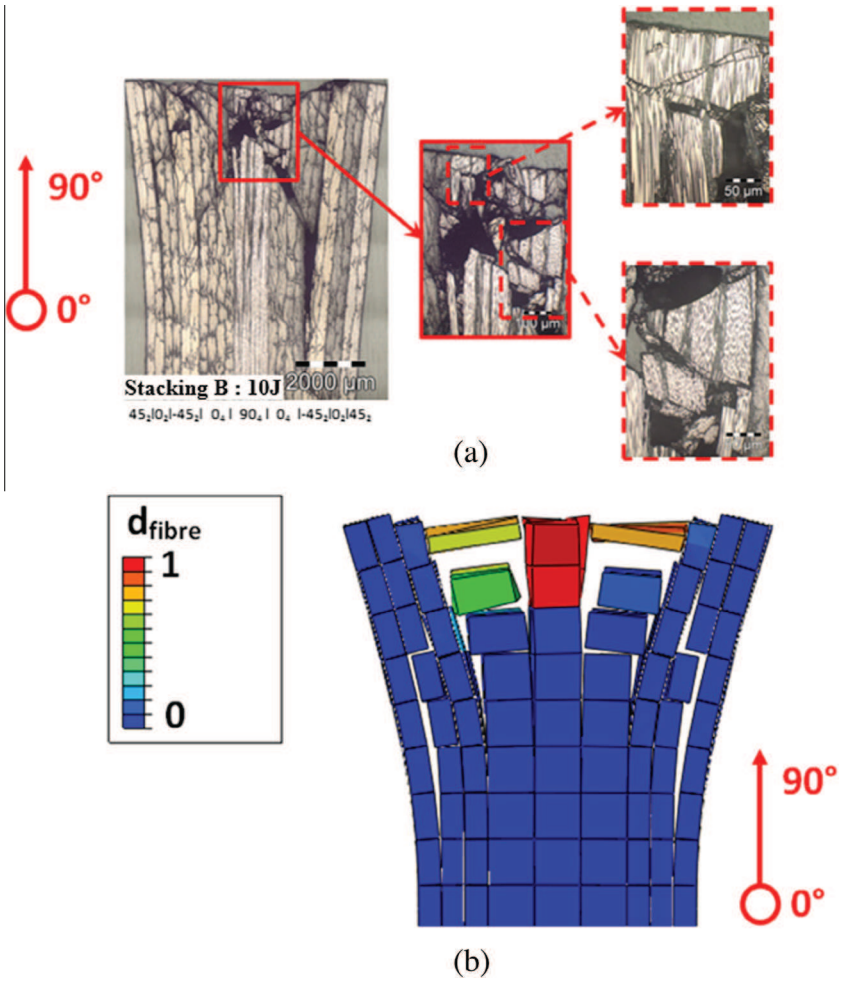

Fig. 16. Microscopic cut section of kink-bands of the stacking B impacted at 10 J (a) and corresponding fiber damage numerically obtained (b).

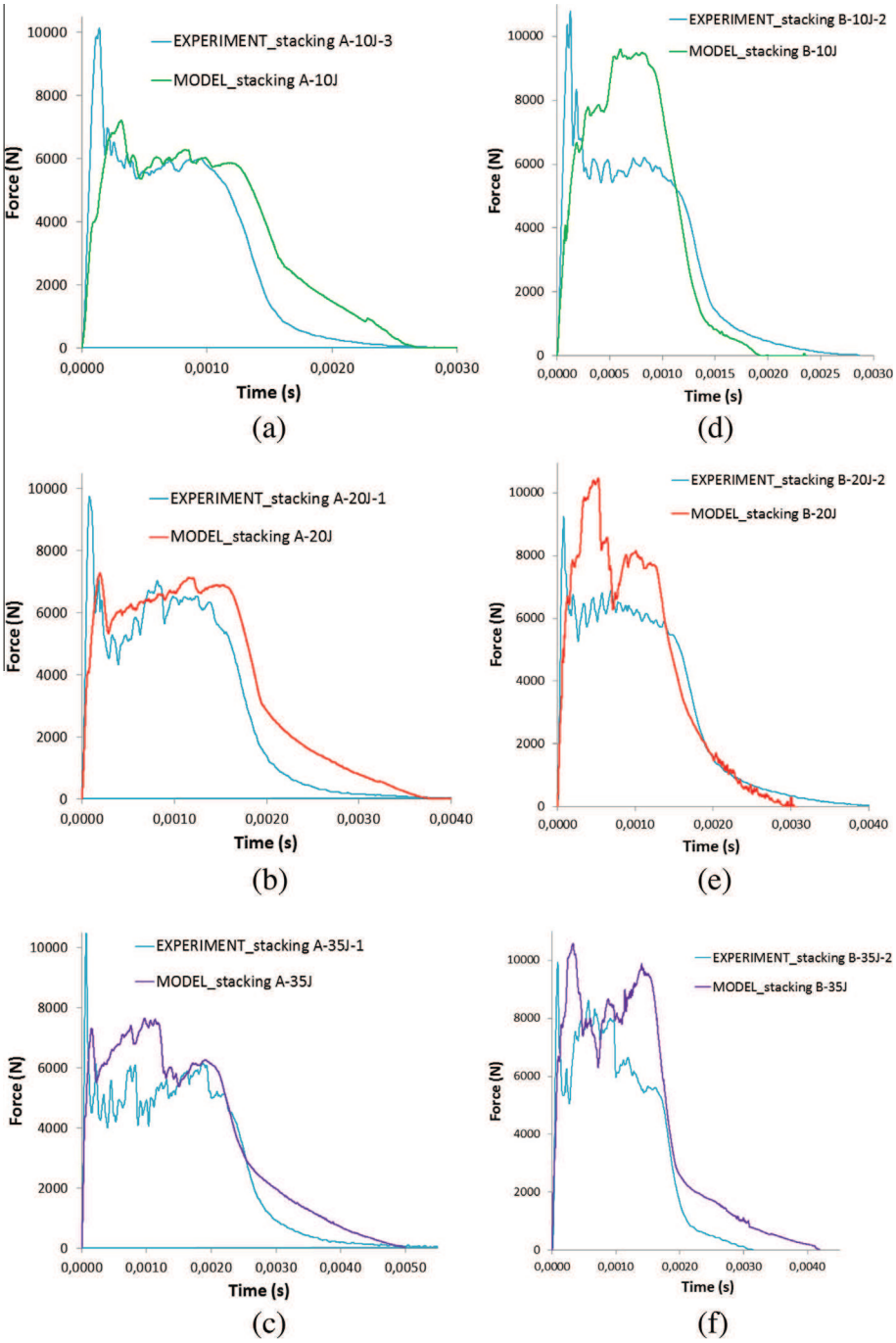

Fig. 17. Experiment/model comparison of the edge impact force/time curves of the stacking A impacted at 10 J (a), 20 J (b) and 35 J (c), and stacking B impacted at 10 J (d), 20 J (e) and 35 J (f).

$$T = N \cdot f \tag{21}$$

The normal force versus tangential force is plotted Fig. 13 for the different fiber orientations.

A similarity of the behavior, whatever the orientation of UD specimen, could be noted with a higher value for 60° and 90° specimens. Due to the low number of experimental tests, it is difficult to conclude with the effect of the fiber orientation on the friction coefficient and thereafter it is supposed constant. In conclusion a friction coefficient of 0.06 is evaluated whatever the fiber orientation; this friction coefficient value will be used in the FE model. This value, although low, is in relative good agreement with the Mondelin et al.'s study [26].

4.2. Edge impact experiment/model comparison

The objective of this paragraph is to test from a qualitative and quantitative point of view the behavior law proposed in the last paragraphs and to compare its results to the edge impact experiments carried out in [16]. The FE model deals with a composite plate of 150 mm-long and 30 mm-high, consisting with the part of the plate outside of the boundary condition during the experiment (Figs. 3 and 14). The bottom part of the plate is clamped and the initial velocity of the 16 mm-diameter and 2.368 kg mass impactor is imposed to obtain the desired impact energy level. The volume element size is fixed to 1 mm-long and 1 mm-width

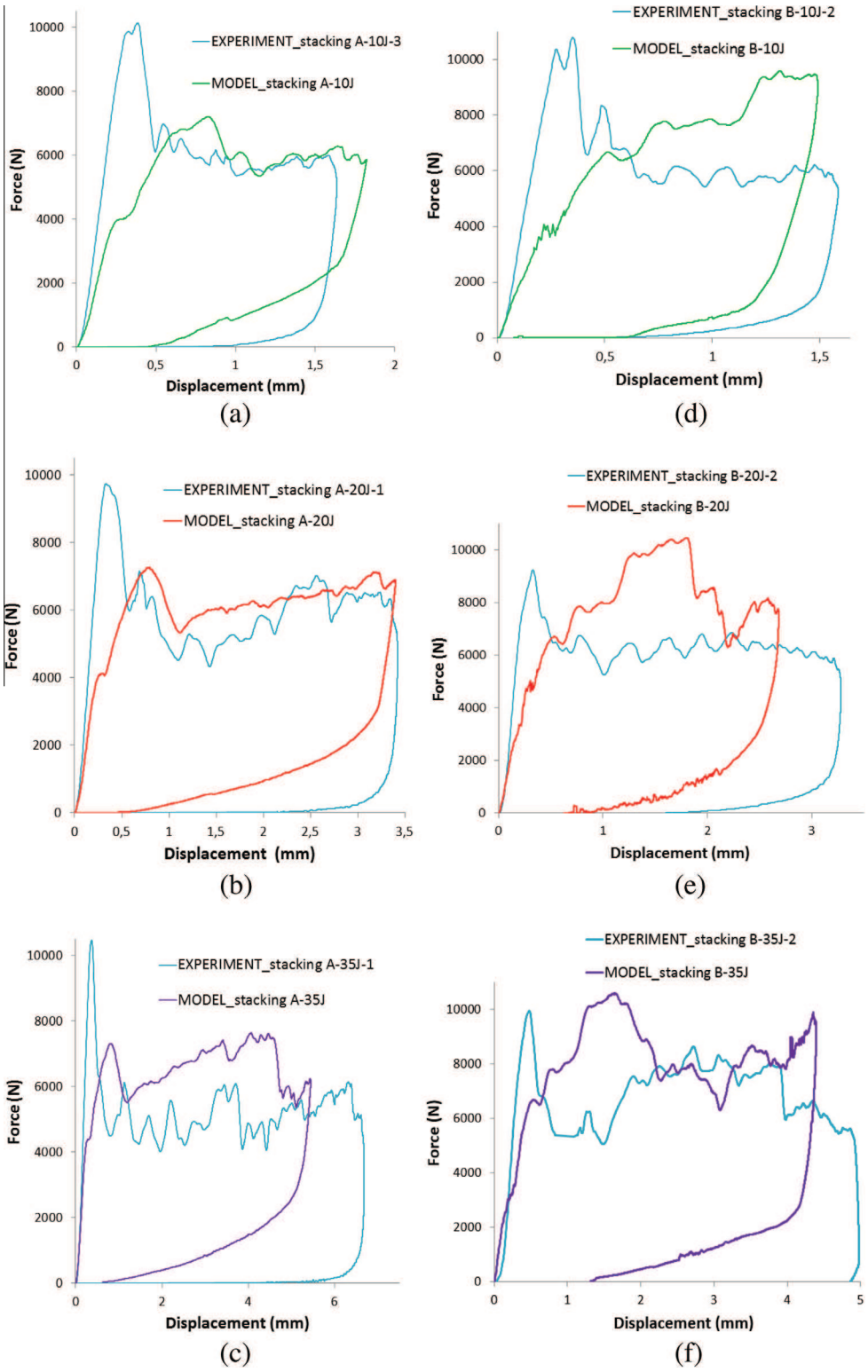

Fig. 18. Experiment/model comparison of the edge impact force/displacement curves of the stacking A impacted at 10 J (a), 20 J (b) et 35 J (c), and stacking B impacted at 10 J (d), 20 J (e) and 35 J (f).

(Fig. 14) to obtain a good representation of the plate avoiding a too long calculation time. One volume element is used for each ply, or more precisely for each plies group in the same direction; that to say 9 plies for stacking A [90_2, -45_2, 0_4, 45_2, 0_4, 45_2, 0_4, -45_2, 90_2] and B [45_2, 0_2, -45_2, 0_4, 90_4, 0_4, -45_2, 0_2, 45_2] (Fig. 15).

An explicit dynamic analysis has been carried out. The cases of stacking A and B impacted at energy level of 10, 20 and 35 J, are presented. After the validation of this edge impact model, the model could directly be applied to the compression after impact modeling; it is the next step of this work.

Experiment/model visual comparison of the damage can be carried out. In particular, the cut sections just under the impactor make it possible to have a first idea of the damage numerically obtained (Fig. 15). It can be noticed in this figure that edge impact

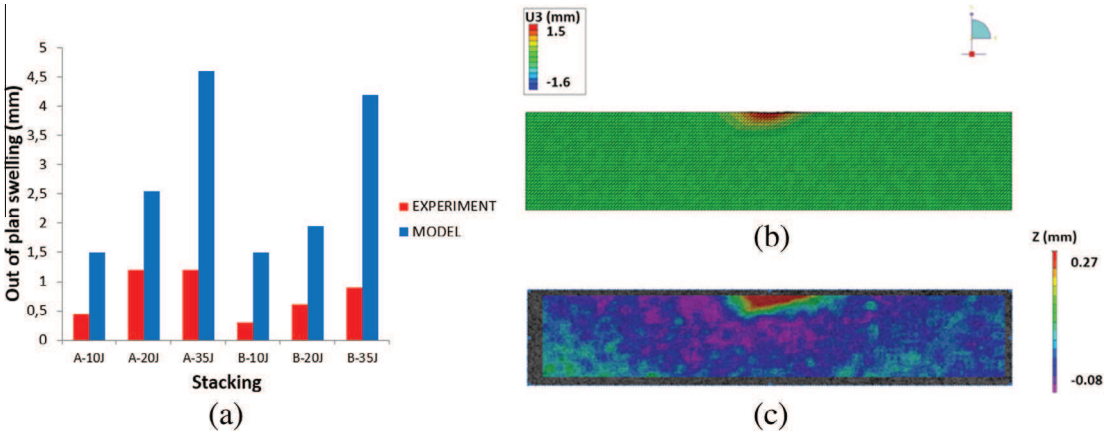

Fig. 19. Experiment/model comparison of the out-of-plan swellings (a) and out-of-plan displacement field numerically (b) and experimentally (c) obtained of the stacking B at 10 J.

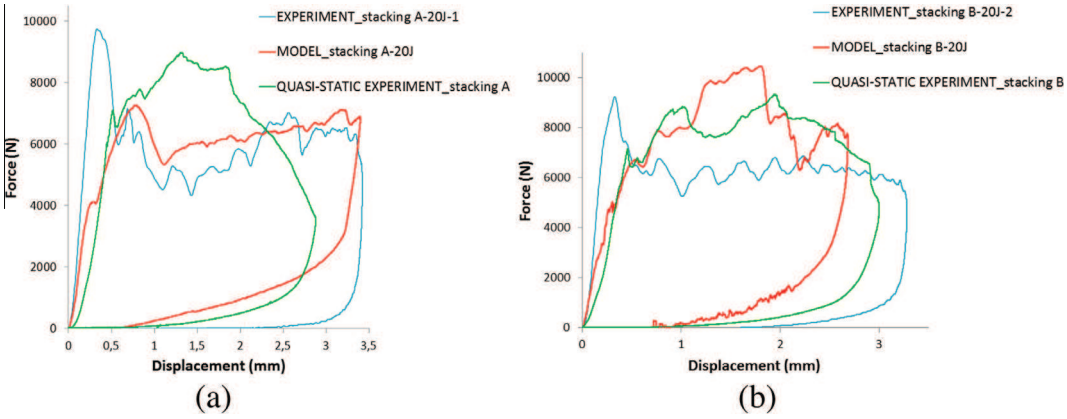

Fig. 20. Experiment/model comparison of the edge impact and edge indentation force/displacement curves of the stacking A impacted at 20 J (a), and stacking B impacted at 20 J (b).

model causes the delamination of all the interfaces as well as the experiment.

It can be noticed using the cut sections of stacking A (Fig. 15a) that the interfaces $90°/-45°^{(1)}$ and $-45°/0°^{(2)}$ are delaminated in the experiment and model. Failure of the offset $0°^{(3)}$ and center $0°^{(4)}$ plies is also qualitatively well simulated. The permanent indentation under the impactor seems also qualitatively well restored. In the case of stacking B (Fig. 15b), the interfaces $45°/0°^{(1)}$ are delaminated on an asymmetrical way in the experiment specimen whereas the model delamination is symmetrical. Delamination of the interfaces $-45°/0°^{(2)}$ seems also numerically underestimated, even if the experimentally obtained delamination is asymmetrical which could explain the discrepancy. Finally the failure of the center $90°^{(3)}$ plies presenting kink-bands on the experiment is well modeled as it can be seen in Fig. 16 where the fiber damage numerically obtained is plotted.

The model thus seems to restore qualitatively fiber failure, matrix cracking and delamination observed during the experiment in an adequate way. From a quantitative point of view the first step to achieve is the study of the force–time curves (Fig. 17).

These curves show an acceptable correlation in terms of total impact time and force fall; the phenomenon is thus more or less well restored in time for the two stacking sequences. It can also be noticed that the maximum force is systematically underestimated for the two stacking sequences. The model of stacking B does not seem to present a force plateau (following the maximum force) such as raised in experiments and this whatever the impact energy level, contrary to the stacking A which presents force plateau similar to the experiment. The second step to achieve consists with the study of the force–displacement curves (Fig. 22).

For the stacking A (Fig. 18a–c), the force increases gradually and reaches a maximum force. Then this force falls and reaches a plateau of a value from approximately 6 kN whatever the impact energy level. The displacement direction of the impactor is finally reversed, the effort falls and a permanent indentation remains. The force–displacement curve of the model is then in relatively good agreement with experiment, even if the force peak is underestimated.

For the stacking B (Fig. 18d–f), the force increases gradually and reaches a maximum force without reaching a crushing plateau. At maximum displacement, there is a sharp fall of the force and a permanent indentation remains. The force–displacement curve of the model is overall in bad agreement with experiment. This discrepancy can be explained by an excessive out-of-plan swelling (Fig. 19a) numerically obtained. Indeed, it lies between two times (stacking A at 20 J; Fig. 19a) and five times (stacking B at 10 J; Fig. 19b and c) the experimental values.

It is interesting to superimpose the force–displacement curves of the model with those of the edge impact and edge indentation (corresponding to quasi-static loading) experiments (Fig. 20).

It can be noticed that the model quickly answers in crushing mode and seems to pass in an inadequate way from the dynamic behavior to the quasi-static behavior. In order to correct this problem it seems necessary to implement a strain rate effect in the

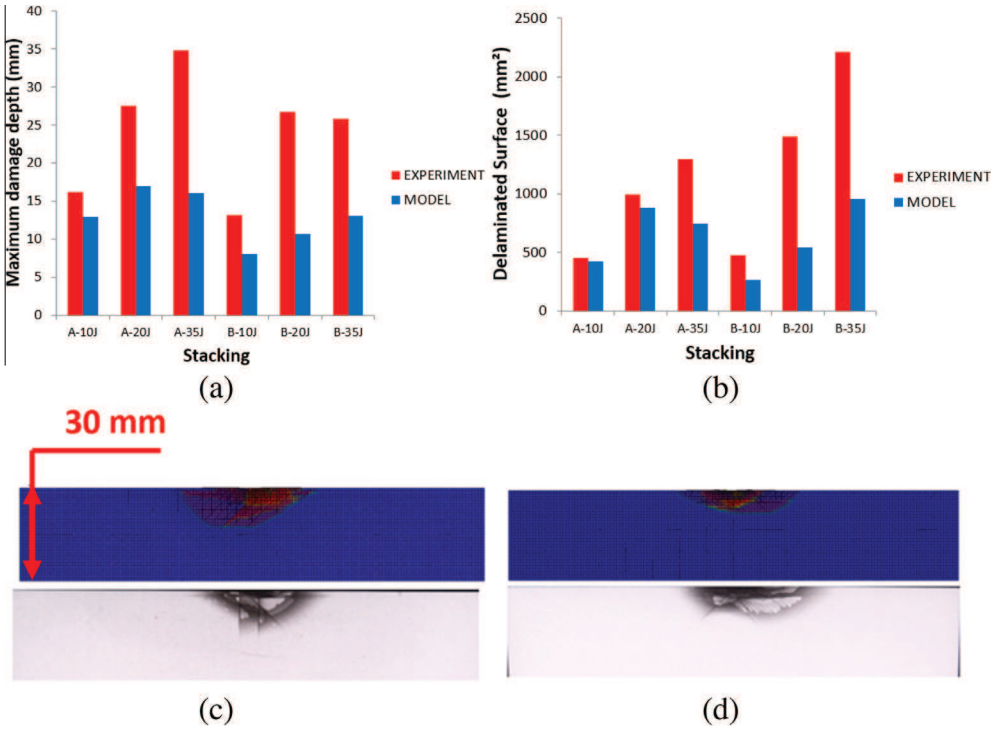

Fig. 21. Experiment/model comparison of the maximum damage depth (a), the projected delaminated area (b) and a model/X-ray comparison of the delaminated surface of the stacking A (c) and B (d) impacted at 10 J.

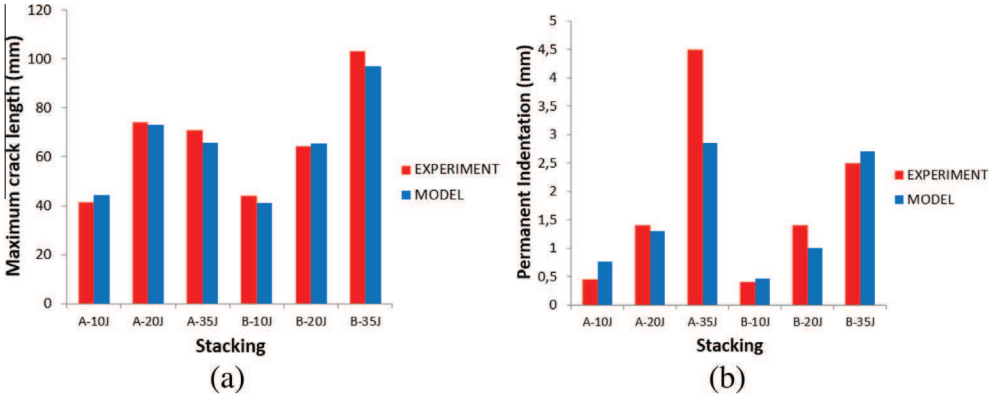

Fig. 22. Experiment/model comparison of maximum crack length on the edge (a) and permanent indentation (b).

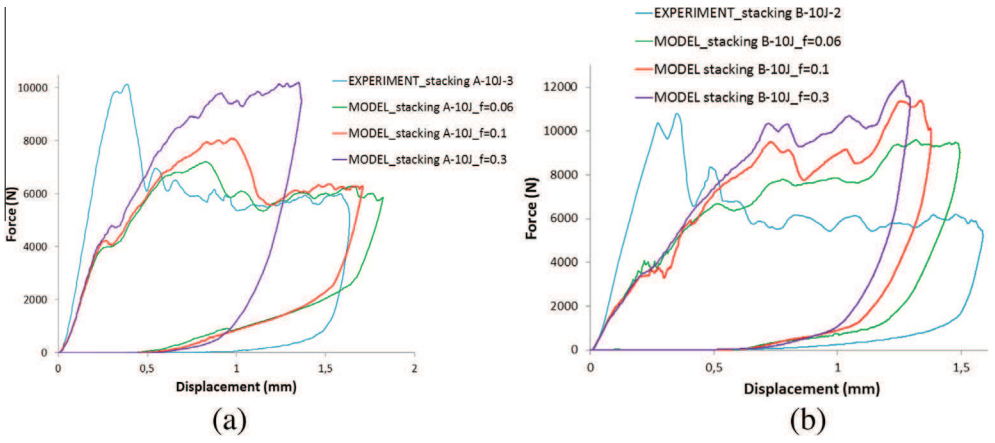

Fig. 23. Experiment/model comparison with different friction coefficients of the edge impact force/displacement curves of the stacking A (a), and B (b) impacted at 10 J.

behavior law of the fiber failure in compression [6,14]. Indeed it has been shown using experimental study [16] that the first force peak of the dynamic edge impact is due to fiber loading until the compressive fiber failure, while the first loading of the quasi-static edge impact is due to crushing process (Fig. 5). Then it will be necessary in the future to take into account more accurately the passage between crushing process and fiber failure, and in particular to account for the strain rate effect in the behavior law of the fiber failure [6,14].

Then the evolution of the maximum damage depth (Fig. 21a) and projected delaminated area (Fig. 21b) can be drawn according to the impact energy stacking.

The projected delaminated area presents a good agreement between experiment and modeling for stacking A whereas modeling of stacking B underestimates this delaminated area of 55% on average. Nevertheless the damage form seems faithful simulated for stacking A (Fig. 21c) and B (Fig. 21d). Finally, a relatively good experiment/modeling agreement is revealed concerning the results of the parameters retained by industry; the maximum crack length on the edge (Fig. 22a) and the permanent indentation (Fig. 22b). Once again, higher is the impact energy, longer the crack is.

4.3. Friction sensitivity

It is interesting to perform a sensitivity study of the friction coefficient using the model and in particular to evaluate the accuracy of the measured value of 0.06. Indeed this very low friction coefficient is close to the value commonly used of 0.1 for a contact between two lubricated surfaces (steel–iron) whereas a value closer to 0.3, commonly used for two dry surfaces (Steel–Cast iron type), could be expected. We thus propose to compare these three values with the edge impact model of the stacking sequences A and B. The force–displacement curves (Fig. 23) clearly make possible to identify the influence of the friction parameter.

It is noticed that the friction coefficient acts particularly on the two results of the edge impact modeling which are the permanent indentation and the maximum force. When the friction coefficient increases, the permanent indentation decreases and the maximum force increases. It is interesting and reassuring to observe the model with a coefficient of friction of 0.06 presents the best experiment–model correlation.

5. Conclusions

This paper presents the major modifications provided to the DPM of [17,18] in order to take into account the crushing process in the fiber and in the transverse direction. Here are the major results of this study:

- From a qualitative and quantitative point of view, edge impact model causes the delamination of all the interfaces as well as the experimental study.
- Kink-bands observed during experiment are relatively well modeled.
- The model seems to restore fiber failure, matrix cracking and delamination during the experiment in an adequate way.
- From a quantitative point of view, the force–time curves show a relatively good correlation in terms of total impact time and force fall; the phenomenon is thus well restored in time for the two stacking sequences.
- The maximum force is systematically underestimated for the two stacking sequences. Then it could be necessary in the future to take into account more accurately the passage between crushing process and fiber failure, and in particular to account for the strain rate effect in the behavior law of the fiber failure [6,14].
- Projected delaminated area presents a good agreement between experiment and modeling for stacking A whereas stacking B underestimates this delaminated area of 55% on average. Nevertheless the damage form seems faithful simulated for stacking A and B.
- Finally, a relatively good experiment/model agreement is revealed concerning the results of the parameters retained by industry; the maximum crack length on the edge and the permanent indentation. Once again, higher is the impact energy, longer the crack is.
- A sensitivity study has been performed to determine the influence of the friction coefficient on the model and to validate the friction coefficient of 0.06. The model with this friction coefficient presents the best experiment–model correlation. The friction phenomenon has an effect on the model results and in particular on the failure form. Part of edge impact model discrepancies could be due to the friction effects.
- It can be noticed that the model quickly answers in crushing mode and seems to pass in an inadequate way from the dynamic behavior to the quasi-static behavior. In order to correct this problem it seems necessary to implement a strain rate effect in the behavior law of the fiber failure in compression. This work will have to be taken into account in the future.

This edge impact model is similar to out-of-plan impact model on a laminate plate [17] with addition of new friction and crushing behaviors. The trends are restored overall but obviously it remains a lot of work to carry out for better restoring the damage scenario and in particular the strain rate effect on the compression and the crushing behaviors. Nevertheless, this model will be applied to the compression after impact model for the moment.

Acknowledgment

This work was granted access to the HPC resources of CALMIP under the allocation 2012-P1026.

References

[1] Abdallah EA, Bouvet C, Rivallant S, Broll B, Barrau J-J. Experimental analysis of damage creation and permanent indentation on highly oriented plates. Compos Sci Technol 2009;69(7–8):1238–45.
[2] Abrate S. Impact on composite structures. Cambridge Univ. Press; 1998. <http://ebooks.cambridge.org/ref/id/CBO9780511574504>.
[3] Aoki Y, Suemasu H, Ishikawa T. Damage propagation in CFRP laminates subjected to low velocity impact and static indentation. Adv Compos Mater 2007:45–61.
[4] Rouchon J. Fatigue and damage tolerance aspects for composite aircraft structures. In: Proceedings of ICAF symposium, Delft; 1995.
[5] Wisnom M. The challenge of predicting failure in composites. In: 19th International conference on composite materials, Montreal, Canada; 2013.
[6] Kaddour AS, Hinton M. Evaluation of theories for predicting failure in polymer composite laminates under 3-D states of stress: Part A of WWFE-II. In: Proceedings of the 19th ICCM. Montréal, Canada; 2013.
[7] Kaddour AS, Hinton M. Maturity of 3D failure criteria for fibre-reinforced composites – Comparison between theories and experiments – Part B of WWFEII. In: Proceedings of the 19th ICCM. Montréal, Canada; 2013.
[8] Kaddour AS, Hinton MJ, Smith PA, Li S. A comparison between the predictive capability of current matrix cracking, continuum damage and fracture criteria for fibre reinforced composite laminates: Part A of WWFE-III. In: Proceedings of the 19th ICCM, Montréal, Canada; 2013.
[9] Malhotra A, Guild FJ, Pavier M. Edge impact to composite laminates – experiments and simulations. J Mater Sci 2008;43(20):6661–7.
[10] Rhead AT, Marchant D, Butler R. Compressive strength of composite laminates following free edge impact. Compos A Appl Sci Manuf 2010;41(9):1056–65.
[11] Choi HY, Chang K. A model for predicting damage in graphite-epoxy laminated composites resulting from low-velocity point impact. J Compos Mater 1992;26(14):2134–69.

[12] Petit S, Bouvet C, Bergerot A, Barrau JJ. Impact and compression after impact experimental study of a composite laminate with a cork thermal shield. Compos Sci Technol 2007;67:3286–99.
[13] Daniel L, Hogg P, Curtis P. The crush behaviour of carbon fibre angle-ply reinforcement and the effect of interlaminar shear strength on energy absorption capability. Compos B Eng 2000:435–40.
[14] Hull D. A unified approach to progressive crushing of fibre-reinforced composite tubes. Compos Sci Technol 1991:377–421.
[15] Israr HA, Rivallant S, Barrau JJ. Experimental investigation on mean crushing stress characterization of carbon–epoxy plies under compressive crushing mode. Compos Struct 2013;96:357–64.
[16] Ostre B, Bouvet C, Lachaud F, Minot C, Aboissiere J. Edge impact damage scenario on stiffened composite structure. J Compos Mater 2014.
[17] Hongkarnjanakul N, Bouvet C. Validation of low velocity impact modelling on different stacking sequences of CFRP laminates and influence of fibre failure. Compos Struct 2013:549–59.
[18] Bouvet C, Rivallant S, Barrau J-J. Low velocity impact modeling in composite laminates capturing permanent indentation. Compos Sci Technol 2012;72(16):1977–88.
[19] Mi Y, Crisfield MA, Davies GAO. Progressive delamination using interface elements. J Compos Mater 1998;32(14):1246–72.
[20] Hashin Z. Failure criteria for unidirectional fibre composites. J Appl Mech 1980;47:329–34.
[21] ASTM D7136D7136M. Standard test method for measuring the damage resistance of a fiber-reinforced polymer matrix composite to a drop-weight impact event.
[22] Yang Q, Cox B. Cohesive models for damage evolution in laminated composites. Int J Fract 2005;133:107–37.
[23] Pinho ST, Robinson P, Iannucci L. Fracture toughness of the tensile and compressive fibre failure modes in laminated composites. Compos Sci Technol December 2005:2069–79.
[24] Raimondo L, Iannucci L, Robinson P, Curtis PT. A progressive failure model for mesh-size-independent FE analysis of composite laminates subject to low-velocity impact damage. Compos Sci Technol 2012;72:624–32.
[25] Bazant ZP, Oh BH. Progressive Carck and band theory for fracture of concrete. Mater Struct 1983;16:155–77.
[26] Mondelin A, Furet B, Rech J. Characterisation of friction properties between a laminated carbon fibres reinforced polymer and a monocrystalline diamond under dry or lubricated conditions. Tribol Int 2010;43(9):1665–73.
[27] Yamaguchi Y. Frottement des plastiques. Techniques de l'ingénieur 1980:1–12.